A Mononuclear Nonheme Iron(IV)−Amido Complex Relevant for the Compound II Chemistry of Cytochrome P450

Xiaoyan Lu,[†] Xiao-Xi Li,[†] Mi Sook Seo,[†] Yong-Min Lee,[†] Martin Clémancey,[‡] Pascale Maldivi,[§] Jean-Marc Latour,[*,‡] Ritimukta Sarangi,[*,∥] Shunichi Fukuzumi,[*,†] and Wonwoo Nam[*,†,⊥]

[†]Department of Chemistry and Nano Science, Ewha Womans University, Seoul 03760, Korea

[‡]Université Grenoble Alpes, CEA, CNRS, BIG, LCBM, Grenoble F-38000, France

[§]Université Grenoble Alpes, CEA, CNRS, INAC, SYMMES, Grenoble F-38000, France

[∥]Stanford Synchrotron Radiation Lightsource, SLAC National Accelerator Laboratory, Stanford, California 94025, United States

[⊥]State Key Laboratory for Oxo Synthesis and Selective Oxidation, Suzhou Research Institute of LICP, Lanzhou Institute of Chemical Physics (LICP), Chinese Academy of Sciences, Lanzhou 730000, China

ABSTRACT: A mononuclear nonheme iron(IV)−amido complex bearing a tetraamido macrocyclic ligand, $[(TAML)Fe^{IV}(NHTs)]^-$ (**1**), was synthesized via a hydrogen atom (H atom) abstraction reaction of an iron(V)−imido complex, $[(TAML)Fe^{V}(NTs)]^-$ (**2**), and fully characterized using various spectroscopies. We then investigated (1) the pK_a of **1**, (2) the reaction of **1** with a carbon-centered radical, and (3) the H atom abstraction reaction of **1**. To the best of our knowledge, the present study reports for the first time the synthesis and chemical properties/reactions of a high-valent iron(IV)−amido complex.

Heme and nonheme iron enzymes as well as their synthetic model compounds catalyze the hydroxylation of alkanes with high efficiency and selectivity.[1−3] High-valent iron(IV)-oxo porphyrin π-cation radical species ($Porp^{+\bullet}$)-$Fe^{IV}(O)$, referred to as compound I (Cpd-I), are the key intermediates responsible for the C−H hydroxylation of substrates in heme systems; a hydrogen atom is abstracted from substrate C−H bonds by Cpd-I (Scheme 1A, reaction *a*),

Scheme 1. C−H Bond Activation Reactions of Cpd-I and Fe(V)−Imido Complex

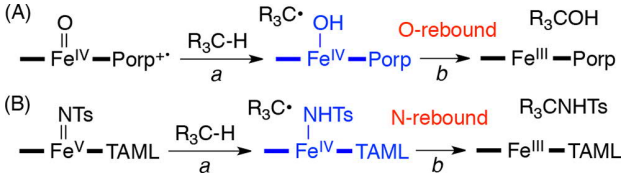

followed by a fast oxygen rebound between the Fe(IV)−OH porphyrin species, referred to as compound II (Cpd-II), and the carbon radical (Scheme 1A, reaction *b*).[1,4] Since the H atom abstraction by Cpd-I is the rate-determining step (rds) (Scheme 1A, reaction *a*), the O-rebound step has never been observed directly (Scheme 1A, reaction *b*). However, very recently, Goldberg and co-workers reported the first direct O-rebound process, in which an iron(IV)−hydroxide corrole complex, $[Fe^{IV}(OH)]$,[5] and a nonheme iron(III)−methoxide complex, $[Fe^{III}(OCH_3)]$,[6] were utilized in reactions with carbon-centered radicals. In the study, they demonstrated the C−O bond formation between Fe−OX (X = H and CH_3) and carbon radicals.[5,6]

Another interesting subject that has attracted much attention recently is the basicity of the Cpd-II Fe(IV)−OH;[1b,7,8] the basicity of the Fe(IV)−OH species is an important factor that determines the reactivity of Cpd-I in C−H activation reactions and that the strong electron-donating ability of the thiolate axial ligand increases the basicity of the iron-oxo moiety, influencing the reactivity of Cpd-I in H atom abstraction reactions. Indeed, pK_as of several Fe(IV)−OH intermediates were determined in heme enzymes,[7,8] showing that Cpd-II with a high pK_a is more reactive in C−H bond activation reactions.

High-valent iron−imido (Fe=NR) and iron−amido (Fe-NHR) species, which are iron−oxo (Fe=O) and iron−hydroxo (Fe−OH) analogs, respectively, have been proposed as reactive intermediates in nitrogen group transfer reactions.[9] Very recently, we reported that a high-valent iron(V)−imido complex, $[(TAML)Fe^{V}(NTs)]^-$ (**2**) (NTs = tosylimido), is capable of activating C−H bonds of substrates (Scheme 1B).[10] In the amination reactions, an iron(IV)−amido intermediate, $[(TAML)Fe^{IV}(NHTs)]^-$ (**1**), is generated as a transient intermediate (Scheme 1B, reaction *a*), as Cpd-II is proposed as a transient intermediate in heme systems (compare Scheme 1A and B). Then, the iron(IV)−amido intermediate is recombined with the carbon radical to yield an aminated product and an iron(III) product (Scheme 1B, reaction *b*). Encouraged by the successful synthesis of the Fe(V)−NTs complex and the reaction of the Fe(V)−NTs complex with alkane C−H bonds,[10a] we attempted to synthesize an Fe(IV)−NHTs complex as an analog of Cpd-II and investigated the chemical properties/reactions of the Fe(IV)−NHTs complex in various aspects. Herein, we report a novel high-valent iron(IV)−amido complex, $[(TAML)Fe^{IV}(NHTs)]^-$ (**1**),

which is synthesized via a H atom abstraction reaction of **2** (Scheme 2, reaction *a*). We also report the pK_a determination, nitrogen rebound, and H atom abstraction reactions of the Fe(IV)−NHTs complex (Scheme 2).

Scheme 2. Schematic Representation for the Synthesis and Reactions of [(TAML)Fe^{IV}(NHTs)]$^-$

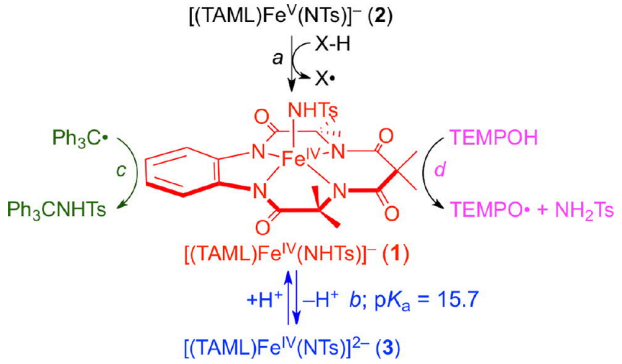

The mononuclear iron(V)−imido complex [(TAML)Fe^{V}(NTs)]$^-$ (**2**) was synthesized according to the literature procedures.[10] Upon addition of 1 equiv of TEMPOH (=2,2,6,6-tetramethylpiperidin-1-ol) or excess amounts of 9,10-dihydroanthracene (DHA) or 1,4-cyclohexadiene (CHD) to **2** in CH_3CN (MeCN) at −40 °C, the color of the reaction solution changed from dark green to purple (Supporting Information (SI), Experimental Section). The purple intermediate (**1**) was metastable ($t_{1/2} \approx 3$ h) at −40 °C, allowing us to characterize it using various spectroscopies, such as UV−vis, cold spray time-of-flight mass spectrometry (CSI-MS), electron paramagnetic resonance (EPR), Mössbauer, and X-ray absorption spectroscopy/extended X-ray absorption fine structure (XAS/EXAFS). The UV−vis spectrum of **1** exhibited two distinct absorption bands at 526 (ε = 6100 M^{-1} cm^{-1}) and 690 nm (ε = 3600 M^{-1} cm^{-1}) (Figure 1a; Figures S1−S3). CSI-MS of **1** in negative mode exhibited a prominent ion peak at *m*/*z* of 596.1, with mass and isotope distribution patterns corresponding to [(TAML)Fe(NHTs)]$^-$ (calculated *m*/*z* of 596.1) (Figure 1a, inset). When **1** was generated using ^{15}N-labeled **2**, [(TAML)Fe^{V}(^{15}NTs)]$^-$, one-mass-unit shift from 596.1 to 597.1 was observed (Figure 1a, inset; Figures S4 and S5, inset). This result demonstrates that **1** contains one NHTs group. The X-band EPR spectrum of **1** was silent when **1** was generated using DHA or CHD (Figure S6). However, when **1** was generated using TEMPOH, the EPR spectrum of the reaction solution showed signals at *g* ∼2.0 from TEMPO• (Figure S7).

1 was also analyzed with Mössbauer spectroscopy (Figure 1b). The spectrum recorded at 80 K without applied magnetic field is constituted by a quadrupole doublet accounting for 97% of the sample iron, with hyperfine parameters consistent with an *S* = 1 Fe(IV) species. This assignment was confirmed by experiments at 4.5 K at 0 and 7 T (Figure S8). A global simulation of all spectra resulted in the following parameters: δ = −0.00 mm s^{-1}, ΔE_Q = 3.33 mm s^{-1}, and *D* = 15 cm^{-1} (Table S1), which match with those reported for other Fe(IV) complexes of related ligands.[11]

Fe K-edge XAS was performed on solutions of **1** and **2**, and the data are presented in Figure 2a. The data show that the rising edge of **1** is ∼1 eV lower in energy relative to **2**. A

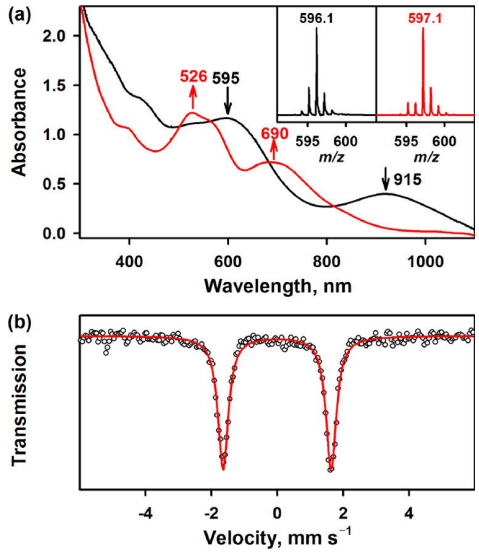

Figure 1. (a) UV−vis spectra of [Fe^{V}(NTs)(TAML)]$^-$ (**2**, black line) and [Fe^{IV}(NHTs)(TAML)]$^-$ (**1**, red line). **1** was synthesized by reacting **2** (0.20 mM) with 1.0 equiv of TEMPOH (0.20 mM) in MeCN at −40 °C. Insets show CSI-MS spectra with the isotopic distribution patterns of the peaks at *m*/*z* 596.1 for **1**-^{14}NHTs (left panel) and at *m*/*z* 597.1 for **1**-^{15}NTs (right panel). (b) Mössbauer spectra (black circles) with fits (red line) for **1** recorded at 80 K and 0 T. The solid line is a calculated spectrum with the following parameters: δ = −0.01 mm s^{-1} and ΔE_Q = 3.28 mm s^{-1}.

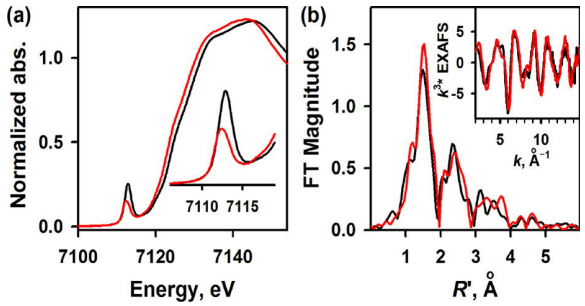

Figure 2. (a) Normalized Fe K-edge XAS data for **1** (red) and **2** (black). The inset shows the expanded pre-edge region. (b) Non-phase-shift-corrected Fourier transform (FT) data for **1** (red) and **2** (black). The inset shows the EXAFS data.

comparison of the pre-edge region is present in the inset of Figure 2a, which shows that the pre-edge energy position of **1** has shifted to lower energy by ∼0.5 eV (7112.9 eV in **2** to 7112.4 eV in **1**), and the intensity has decreased significantly in **1** relative to **2**. This lowering of pre-edge energy position and decrease in intensity suggest a change in the Fe−N axial interaction on going from **2** to **1**.[10b,12,13] Fe K-edge EXAFS data for **1** and **2** were measured and analyzed for local structure determination. A comparison is shown in Figure 2b, and fits to the data of **1** are shown in Figure S9 and Table S2. The best fits to the data for **1** reveal a first shell devoid of a short Fe−N interaction and consistent with either four or five Fe−N interactions at 1.89 Å (Table S2), suggesting elongation of the Fe−N relative to **2**. These data are supported by TD-DFT simulations of the Fe K-edge pre-edge region on the triplet ground state structure of a five-coordinate **1** and comparing that to that of **2**. The TD-DFT calculations (Figure S10) reveal an excellent agreement with the Fe K-pre-edge

data, supporting the five-coordinate EXAFS fit. Based on the spectroscopic characterization and the density functional theory (DFT) calculations (see Figure S11 for the DFT-optimized structure; Table S3), **1** can be assigned as an $S = 1$ iron(IV)−amido complex with a single Fe−N bond, $[(TAML)Fe^{IV}(NHTs)]^-$.

We then investigated the pK_a of Fe(IV)-N(H)Ts by the spectroscopic titration with bases in MeCN at −40 °C (Scheme 2, reaction *b*). When **1** was reacted with pyridine (pK_a = 12.3)[14] and 2-aminopyridine (pK_a = 14.3),[14] we did not observe any spectral changes in the reactions. However, addition of 1 equiv of 4-dimethylaminopyridine (4-DMAPy, pK_a = 17.6)[14] or 4-aminopyridine (4-APy, pK_a = 17.2)[14] to **1** resulted in the fast disappearance of the peaks at 526 and 690 nm due to **1** with the formation of a new species (**3**) (Figures S12 and S13). Interestingly, addition of 1 equiv of HOTf to the solution of **3** regenerated **1** (Figure S14) (Scheme 2, reaction *b*). Thus, the results of the acid−base reaction indicate that addition of base to **1** generates a deprotonated species, $[(TAML)Fe^{IV}(NTs)]^{2-}$ (**3**), and **3** is converted back to **1** upon protonation (Scheme 2, reaction *b*). Since **3** is not stable ($t_{1/2}$ ≈ 550 s at −40 °C) (Figure S15) due to disproportionation to $[(TAML)Fe^{V}(NTs)]^-$ and $[Fe^{III}(TAML)]^-$ (Figure S16), we were not able to provide strong spectroscopic evidence for **3** except the UV−vis and EPR data. Indeed, such disproportion reaction of Fe(IV) to Fe(V) and Fe(III) is well documented in iron(IV)-oxo porphyrin chemistry.[15]

Then, the *K* values of the deprotonation of **1** with 4-DMAPy and 4-APy were determined by fitting of the titration data (see SI, Experimental Section and Figures S17−S20). The pK_a of **1** was then determined to be 15.7(1) with the *K* values and the pK_as of 4-DMAPy and 4-APy (eq 1). In addition, with the determined pK_a value of **1**, the BDE value of Fe−N(H)Ts in **1** was also determined to be 79.3 kcal mol^{-1} from the E_{red} value (vs Fc^+/Fc) of **2** using eq 2,[16] where E_{red} (vs Fc^+/Fc) of **2** = −0.07 V (Figure S21). **1** is less basic with the lower BDE than those of $L^{mes}Fe^{III}$−N(H)Ad$^+$, an iron(III)−amido with pK_a = 37 and BDE = 88(5) kcal mol^{-1}, which may result from several factors including the nature of the amide substituent, Fe oxidation state, and charge of the complex.[17]

$$pK_{a,(\mathbf{1})} = -\log K + pK_{a,(4\text{-X-Py})} \quad (1)$$

$$BDE = 1.37pK_{a,(\mathbf{1})} + 23.06E_{red} + 59.4 \quad (2)$$

With the spectroscopically well characterized **1** and **2**, we investigated the H atom abstraction reaction of **2** (Scheme 1B, reaction *a*) and the N-rebound reaction of **1** (Scheme 1B, reaction *b*); triphenylmethane (Ph_3CH) was used as a substrate. First, the reaction of **2** with Ph_3CH yielded $[Fe^{III}(TAML)]^-$ and Ph_3C-NHTs (Figures S22−S24). The second-order rate constant of the reaction of **2** with Ph_3CH was determined at different temperatures and then extrapolated to −40 °C (Figures S25−S27),[18] in which the second-order rate constant was determined to be 7.5×10^{-5} M^{-1} s^{-1} at −40 °C (Scheme 1B, reaction *a*). Then, we examined the N-rebound reaction of **1** with triphenylmethyl radical ($Ph_3C^\bullet$) (Scheme 1B, reaction *b*; also see Scheme 2, reaction *c*). Addition of $(Ph_3C)_2$, which is in equilibrium with $Ph_3C^\bullet$,[19] to a deaerated MeCN solution of **1** at −40 °C under an Ar atmosphere afforded the Ph_3C-NHTs and $[Fe^{III}(TAML)]^-$ products in ∼90% yield (Figures S28 and S29). The rate constant of the N-rebound reaction between **1** and $Ph_3C^\bullet$ at −40 °C was estimated to be larger than 2.4×10^3 M^{-1} s^{-1} from the first-order rate constant (7.2×10^{-3} s^{-1}) in Figure S30, inset, and the maximum concentration of $[Ph_3C^\bullet]$ ($<3 \times 10^{-6}$ M) in the equilibrium with $(Ph_3C)_2$.[20] Thus, by comparing the rate constants of the H atom abstraction of Ph_3CH by **2** (7.5×10^{-5} M^{-1} s^{-1}) and the N-rebound reaction between **1** and $Ph_3C^\bullet$ (2.4×10^3 M^{-1} s^{-1}), we can conclude that the N-rebound reaction (Scheme 1B, reaction *b*) is more than 3.2×10^7 times faster than the H atom abstraction reaction (Scheme 1B, reaction *a*).

Finally, the reaction of **1** with TEMPOH (BDE of O−H = 70.6 kcal mol^{-1})[16c] was investigated (Scheme 2, reaction *d*). Addition of TEMPOH to **1** in MeCN at −40 °C resulted in the disappearance of **1** (Figure S31). The second-order rate constant (k_2) was determined to be 1.6×10^2 M^{-1} s^{-1} at −40 °C (Figure S32). Product analysis revealed the formation of NH_2Ts and $TEMPO^\bullet$ with the yields of ∼95% and ∼86%, respectively, as the organic products (Figures S33 and S34) and the formation of $[Fe^{III}(TAML)]^-$ as the decay product of **1** (Figure S35); the overall reaction stoichiometry is shown in eq 3.

$$[(TAML)Fe^{IV}(NHTs)]^- (\mathbf{1}) + TEMPOH \rightarrow [(TAML)Fe^{III}]^- + NH_2Ts + TEMPO\cdot \quad (3)$$

In summary, we have reported the synthesis and characterization of a mononuclear nonheme iron(IV)−amido complex, $[(TAML)Fe^{IV}(NHTs)]^-$ (**1**). We have also reported the chemical properties and reactions of the iron(IV)−amido complex, such as the pK_a and BDE values and the N-rebound and H atom abstraction reactions.

AUTHOR INFORMATION

Corresponding Authors

*jean-marc.latour@cea.fr
*ritis@slac.stanford.edu
*fukuzumi@chem.eng.osaka-u.ac.jp
*wwnam@ewha.ac.kr

ORCID

Yong-Min Lee: 0000-0002-5553-1453
Ritimukta Sarangi: 0000-0002-2764-2279
Shunichi Fukuzumi: 0000-0002-3559-4107
Wonwoo Nam: 0000-0001-8592-4867

Notes

The authors declare no competing financial interest.

ACKNOWLEDGMENTS

This work was supported by the NRF of Korea through CRI (NRF-2012R1A3A2048842). P.M. thanks GENCI for HPC resources (Grant A0040807648). J.-M.L. and P.M. thank the French National Agency for Research (ANR; ARCANE project no. ANR-11-LABX-003). The SSRL SMB resource was supported by an NIH P41 Resource grant (P41GM103393) and by the DOE Office of Biological and Environmental Research.

REFERENCES

(1) (a) Huang, X.; Groves, J. T. Oxygen Activation and Radical Transformations in Heme Proteins and Metalloporphyrins. *Chem. Rev.* **2018**, *118*, 2491−2553. (b) Yosca, T. H.; Ledray, A. P.; Ngo, J.; Green, M. T. A New Look at the Role of Thiolate Ligation in Cytochrome P450. *J. Biol. Inorg. Chem.* **2017**, *22*, 209−220. (c) Yosca, T. H.; Green, M. T. Preparation of Compound I in $P450_{cam}$: The Prototypical P450. *Isr. J. Chem.* **2016**, *56*, 834−840. (d) Ortiz de Montellano, P. R. Hydrocarbon Hydroxylation by Cytochrome P450 Enzymes. *Chem. Rev.* **2010**, *110*, 932−948. (e) Shaik, S.; Cohen, S.; Wang, Y.; Chen, H.; Kumar, D.; Thiel, W. P450 Enzymes: Their Structure, Reactivity, and Selectivity-Modeled by QM/MM Calculations. *Chem. Rev.* **2010**, *110*, 949−1017.

(2) (a) Solomon, E. I.; Goudarzi, S.; Sutherlin, K. D. O_2 Activation by Non-Heme Iron Enzymes. *Biochemistry* **2016**, *55*, 6363−6374. (b) Kal, S.; Que, L. Dioxygen Activation by Nonheme Iron Enzymes with the 2-His-1-Carboxylate Facial Triad that Generate High-Valent Oxoiron Oxidants. *J. Biol. Inorg. Chem.* **2017**, *22*, 339−365.

(3) (a) Nam, W.; Lee, Y.-M.; Fukuzumi, S. Hydrogen Atom Transfer Reactions of Mononuclear Nonheme Metal−Oxygen Intermediates. *Acc. Chem. Res.* **2018**, *51*, 2014−2022. (b) Engelmann, X.; Monte-Pérez, I.; Ray, K. Oxidation Reactions with Bioinspired Mononuclear Non-Heme Metal-Oxo Complexes. *Angew. Chem., Int. Ed.* **2016**, *55*, 7632−7649. (c) Puri, M.; Que, L., Jr. Toward the Synthesis of More Reactive S = 2 Non-Heme Oxoiron(IV) Complexes. *Acc. Chem. Res.* **2015**, *48*, 2443−2452. (d) Cook, S. A.; Borovik, A. S. Molecular Designs for Controlling the Local Environments around Metal Ions. *Acc. Chem. Res.* **2015**, *48*, 2407−2414. (e) Nam, W.; Lee, Y.-M.; Fukuzumi, S. Tuning Reactivity and Mechanism in Oxidation Reactions by Mononuclear Nonheme Iron(IV)-Oxo Complexes. *Acc. Chem. Res.* **2014**, *47*, 1146−1154.

(4) (a) Huang, X.; Groves, J. T. Beyond Ferryl-Mediated Hydroxylation: 40 Years of the Rebound Mechanism and C−H Activation. *J. Biol. Inorg. Chem.* **2017**, *22*, 185−207. (b) Cho, K.-B.; Hirao, H.; Shaik, S.; Nam, W. To Rebound or Dissociate? This is the Mechanistic Question in C−H Hydroxylation by Heme and Nonheme Metal−Oxo Complexes. *Chem. Soc. Rev.* **2016**, *45*, 1197−1210.

(5) Zaragoza, J. P. T.; Yosca, T. H.; Siegler, M. A.; Moënne-Loccoz, P.; Green, M. T.; Goldberg, D. P. Direct Observation of Oxygen Rebound with an Iron-Hydroxide Complex. *J. Am. Chem. Soc.* **2017**, *139*, 13640−13643.

(6) Pangia, T. M.; Davies, C. G.; Prendergast, J. R.; Gordon, J. B.; Siegler, M. A.; Jameson, G. N. L.; Goldberg, D. P. Observation of Radical Rebound in a Mononuclear Nonheme Iron Model Complex. *J. Am. Chem. Soc.* **2018**, *140*, 4191−4194.

(7) (a) Green, M. T.; Dawson, J. H.; Gray, H. B. Oxoiron(IV) in Chloroperoxidase Compound II Is Basic: Implications for P450 Chemistry. *Science* **2004**, *304*, 1653−1656. (b) Yosca, T. H.; Rittle, J.; Krest, C. M.; Onderko, E. L.; Silakov, A.; Calixto, J. C.; Behan, R. K.; Green, M. T. Iron(IV)hydroxide pK_a and the Role of Thiolate Ligation in C−H Bond Activation by Cytochrome P450. *Science* **2013**, *342*, 825−829. (c) Krest, C. M.; Silakov, A.; Rittle, J.; Yosca, T. H.; Onderko, E. L.; Calixto, J. C.; Green, M. T. Significantly Shorter Fe−S Bond in Cytochrome P450-I is Consistent with Greater Reactivity Relative to Chloroperoxidase. *Nat. Chem.* **2015**, *7*, 696−702. (d) Onderko, E. L.; Silakov, A.; Yosca, T. H.; Green, M. T. Characterization of a Selenocysteine-Ligated P450 Compound I Reveals Direct Link between Electron Donation and Reactivity. *Nat. Chem.* **2017**, *9*, 623−628.

(8) (a) Yosca, T. H.; Langston, M. C.; Krest, C. M.; Onderko, E. L.; Grove, T. L.; Livada, J.; Green, M. T. Spectroscopic Investigations of Catalase Compound II: Characterization of an Iron(IV) Hydroxide Intermediate in a Non-Thiolate-Ligated Heme Enzyme. *J. Am. Chem. Soc.* **2016**, *138*, 16016−16023. (b) Wang, X.; Ullrich, R.; Hofrichter, M.; Groves, J. T. Heme-Thiolate Ferryl of Aromatic Peroxygenase is Basic and Reactive. *Proc. Natl. Acad. Sci. U. S. A.* **2015**, *112*, 3686−3691.

(9) (a) Che, C.-M.; Lo, V. K.-Y.; Zhou, C.-Y.; Huang, J.-S. Selective Functionalisation of Saturated C−H Bonds with Metalloporphyrin Catalysts. *Chem. Soc. Rev.* **2011**, *40*, 1950−1975. (b) Saouma, C. T.; Peters, J. C. M≡E and M=E Complexes of Iron and Cobalt that Emphasize Three-Fold Symmetry (E≡O, N, NR). *Coord. Chem. Rev.* **2011**, *255*, 920−937. (c) Eikey, R. A.; Abu-Omar, M. M. Nitrido and Imido Transition Metal Complexes of Groups 6−8. *Coord. Chem. Rev.* **2003**, *243*, 83−124. (d) Berry, J. F. Terminal Nitrido and Imido Complexes of the Late Transition Metals. *Comments Inorg. Chem.* **2009**, *30*, 28−66. (e) Zhang, L.; Deng, L. C-H Bond Amination by Iron-Imido/Nitrene Species. *Chin. Sci. Bull.* **2012**, *57*, 2352−2360.

(10) (a) Hong, S.; Sutherlin, K. D.; Vardhaman, A. K.; Yan, J. J.; Park, S.; Lee, Y.-M.; Jang, S.; Lu, X.; Ohta, T.; Ogura, T.; Solomon, E. I.; Nam, W. A Mononuclear Nonheme Iron(V)-Imido Complex. *J. Am. Chem. Soc.* **2017**, *139*, 8800−8803. (b) Hong, S.; Lu, X.; Lee, Y.-M.; Seo, M. S.; Ohta, T.; Ogura, T.; Clémancey, M.; Maldivi, P.; Latour, J.-M.; Sarangi, R.; Nam, W. Achieving One-Electron Oxidation of a Mononuclear Nonheme Iron(V)-Imido Complex. *J. Am. Chem. Soc.* **2017**, *139*, 14372−14375.

(11) Collins, T. J.; Fox, B. G.; Hu, Z. G.; Kostka, K. L.; Münck, E.; Rickard, C. E. F.; Wright, L. J. High Valent Transition Metal Chemistry. Synthesis and Characterization of an Intermediate-Spin Iron(IV) Complex of a Strong π-Acid Ligand. *J. Am. Chem. Soc.* **1992**, *114*, 8724−8725.

(12) Sarangi, R. X-ray Absorption Near-Edge Spectroscopy in Bioinorganic Chemistry: Application to M−O_2 Systems. *Coord. Chem. Rev.* **2013**, *257*, 459−472.

(13) Westre, T. E.; Kennepohl, P.; DeWitt, J. G.; Hedman, B.; Hodgson, K. O.; Solomon, E. I. A Multiplet Analysis of Fe K-Edge 1s → 3d Pre-Edge Features of Iron Complexes. *J. Am. Chem. Soc.* **1997**, *119*, 6297−6314.

(14) Spillane, W. J.; O'Byrne, A.; McCaw, C. J. A. Elimination Mechanisms in the Aminolysis of Sulfamate Esters of the Type $NH_2SO_2OC_6H_4X$ − Models of Enzyme Inhibitors. *Eur. J. Org. Chem.* **2008**, *2008*, 4200−4205.

(15) (a) Pan, Z.; Newcomb, M. Kinetics and Mechanism of Oxidation Reactions of Porphyrin-Iron(IV)-Oxo Intermediates. *Inorg. Chem.* **2007**, *46*, 6767−6774. (b) Pan, Z.; Newcomb, M. Acid-Catalyzed Disproportionation of Oxoiron(IV) Porphyrins to Give Oxoiron(IV) Porphyrin Radical Cations. *Inorg. Chem. Commun.* **2011**, *14*, 968−970.

(16) (a) Mayer, J. M. Hydrogen Atom Abstraction by Metal−Oxo Complexes: Understanding the Analogy with Organic Radical Reactions. *Acc. Chem. Res.* **1998**, *31*, 441−450. (b) Green, M. T. C−H Bond Activation in Heme Proteins: The Role of Thiolate Ligation in Cytochrome P450. *Curr. Opin. Chem. Biol.* **2009**, *13*, 84−88. (c) Warren, J. J.; Tronic, T. A.; Mayer, J. M. Thermochemistry of Proton-Coupled Electron Transfer Reagents and its Implications. *Chem. Rev.* **2010**, *110*, 6961−7001.

(17) Nieto, I.; Ding, F.; Bontchev, R. P.; Wang, H.; Smith, J. M. Thermodynamics of Hydrogen Atom Transfer to a High-Valent Iron Imido Complex. *J. Am. Chem. Soc.* **2008**, *130*, 2716−2717.

(18) The rate constant of hydrogen atom transfer from triphenylmethane to **2** has been included in the previously reported plot of log k_2' vs BDEs of substrates (ref 10a) at 15 °C in the SI, Figure S27.

(19) (a) Colle, T. H.; Glaspie, P. S.; Lewis, E. S. The Triphenylmethyl Radical: Equilibrium Measurements and the Reaction with Thiophenol. *J. Org. Chem.* **1978**, *43*, 2722−2725. (b) Jang, E. S.; McMullin, C. L.; Käß, M.; Meyer, K.; Cundari, T. R.; Warren, T. H. Copper(II) Anilides in sp^3 C-H Amination. *J. Am. Chem. Soc.* **2014**, *136*, 10930−10940. (c) Iovan, D. A.; Betley, T. A. Characterization of Iron-Imido Species Relevant for N-Group Transfer Chemistry. *J. Am. Chem. Soc.* **2016**, *138*, 1983−1993.

(20) The concentration of $Ph_3C^\bullet$ during the reaction was too small to be detected, being estimated to be smaller than 3×10^{-6} M from ΔA (<0.001) based on the ε value at 514 nm due to $Ph_3C^\bullet$ (SI, Experimental Section). The reaction of **1** with $Ph_3C^\bullet$ was much faster than the formation of $Ph_3C^\bullet$ from the dimer (SI, Figure S30).